MIT Libraries | DSpace@MIT

MIT Open Access Articles

Effect of sequence features on assembly of spider silk block copolymers

Massachusetts Institute of Technology

Effect of Sequence Features on Assembly of Spider Silk Block Copolymers

Olena S. Tokareva[1], **Shangchao Lin**[2], **Matthew M. Jacobsen**[3], **Wenwen Huang**[1,4], **Daniel Rizzo**[4], **David Li**[3], **Marc Simon**[4], **Cristian Staii**[4], **Peggy Cebe**[4], **Joyce Y. Wong**[3], **Markus J. Buehler**[2], and **David L. Kaplan**[1]

[1]Department of Biomedical Engineering, Tufts University, Medford, MA 02155

[2]Department of Civil and Environmental Engineering, Massachusetts Institute of Technology, Cambridge, MA 02139

[3]Department of Biomedical Engineering, Division of Materials Science and Engineering,, Boston University, Boston, MA 02215

[4]Department of Physics and Astronomy, Center for Nanoscopic Physics, Tufts University, Medford, MA 02155

Abstract

Bioengineered spider silk block copolymers were studied to understand the effect of protein chain length and sequence chemistry on the formation of secondary structure and materials assembly. Using a combination of *in vitro* protein design and assembly studies, we demonstrate that silk block copolymers possessing multiple repetitive units self-assemble into lamellar microstructures. Additionally, the study provides insights into the assembly behavior of spider silk block copolymers in concentrated salt solutions.

Introduction

Spider silk motifs and their structure-function relationships have been a focus of research for almost two decades, due to the outstanding mechanical and biophysical properties of these protein fibers and their origins in an all aqueous, ambient spinning environment (An et al., 2012; Tokareva et al., 2013b). Spider silks are remarkable natural polymers that consist of distinct peptide domains: repetitive middle core domains and two non-repetitive N-terminal and C-terminal domains (Bini et al., 2004). At least seven different types of silk proteins are known for some orb-weaving spiders (Lewis, 2006). These silks differ in primary sequence, physical properties and functions depending on the source species and the specific type of silk, as spiders use silk to build orb web frames and radii, for lifelines and for anchoring to

substrates (Gosline et al., 1984). Spiders produce superior protein fibers compared to a well-known silkworm *Bombyx mori* (Lewis, 2006). Silk threads made of the major ampullate silks have a tensile strength (the maximum stress that a material can withstand while being stretched or pulled before failing or breaking) higher than steel and comparable to Kevlar, a material used in a bullet proof vests, and modest elasticity (Gosline et al., 1999). The exceptional mechanical properties of these spider silk fibers have inspired research into generating these proteins via recombinant DNA approaches in order to study material properties *in vitro*. In addition to engineering recombinant silk fibers, material scientists are interested in self-assembly of silk proteins into non-natural (non-fiber) material formats such as microspheres, films, hydrogels, and microcapsules.

The large core peptide domains in spider dragline silks are generally organized in block copolymer-like arrangements, in which two peptide sequences, crystalline (poly(A) and/or poly(GA)) and less crystalline (GGX or GPGXX) polypeptides alternate (Tokareva et al., 2013b). The principles of the block copolymer designs from the study of synthetic polymers served as a guide for these protein systems, based on the sequence of the major ampullate dragline silk I (MaSp I) of the golden orb weaver, *Nephila clavipes*. Moreover, spider silks are useful models to study the relationship between amino acid sequences, block distributions and compositions, chain length, and functional properties such as mechanics. Predicting block copolymer self-assembly behavior *in vitro* is challenging. Such experimental techniques are important to provide insight into block copolymer behavior, yet insight into mechanisms that govern self-assembly of these types of structural proteins remains limited. The complexity of the self-assembly processes with multiblock copolymers, in particular proteins, is also exacerbated by the lack of theories to describe the morphology and structure from sequence data, except for the simplest synthetic diblock copolymers (Mai and Eisenberg, 2012). For example, the Flory-Huggins parameter (χ_{AB}) is typically used to quantify the degree of incompatibility between the hydrophobic and hydrophilic blocks or domains. However, phase diagram predictions using the self-consistent mean-field (SCMF) theory and χ_{AB} parameters are still limited to diblock or triblock copolymers in bulk without solvents (Matsen and Schick, 1994). Therefore, advanced simulation approaches can fill the gap between experimental and theoretical studies with more complicated copolymers, such as those described in this work. This need is amplified with proteins, where complexity in sequence chemistry due to the 20 different amino acid chemistries, combined with the role of an aqueous environment, prohibit simple design rules and facile identification of fundamental rules that govern self-assembly.

Previously, we demonstrated the role of poly(alanine) distributions on β-sheet formation in spider silk block copolymers, using Fourier transform infrared spectroscopy (FTIR) and wide angle X-ray scattering (WAXS) to demonstrate that the number of poly(A) domains had a direct influence on the formation of crystalline β-sheets (Rabotyagova et al., 2010). In the present study, the goal was to understand the effect of peptide block length on the propensity to support self-assembly, a key step in formation of functional materials. Two different spider silk block copolymer designs were studied to provide this insight, copolymers H(AB)$_2$ and H(AB)$_{12}$. Here the A block is composed of a hydrophobic β-sheet forming poly(A) sequence, the B block consists of four hydrophilic GGX repeats, and the H

block (a histidine tag) is made of six histidine residues and a short linker sequence to facilitate the purification of the recombinant proteins. In addition to the experimental approach to study assembly, a computational modeling tool based on coarse-grained (CG) dissipative particle dynamic (DPD) simulations (Groot and Warren, 1997) was employed to predict spherical aggregates formation *in silico* for comparisons to the experimental data. The DPD model is a representative CG approach that has been widely applied to study the structural evolution of polymer solutions. The results suggest that in addition to β-sheet content, the number of blocks (repeats) in a spider silk-like copolymer (e.g., polymer chain length), is an essential parameter that needs to be considered for successful materials formation.

Materials and Methods

Materials

The pET30a(+) vector was obtained from Novagen (Madison, WI). Synthetic oligonucleotides were purchased from Invitrogen (Carlsbad, CA). Restriction enzymes, calf intestinal phosphatase (CIP), T4 ligase, and Quick ligation kits were purchased from New England Biolabs (Beverley, MA). DNA purification was performed using kits from Qiagen (Valencia, CA). Ninitrilotriacetic acid (Ni-NTA)-agarose resin for protein purification was acquired from Qiagen (Valencia, CA). Slide-A-Lyzer dialysis cassettes were obtained from Pierce (Rockford, IL). The 1kb DNA ladder, NuPAGE 4–12% Bis-tris protein gels, SeeBlue Plus 2 protein standard, and T1 phage-resistant cells were purchased from Invitrogen (Carlsbad, CA). All cloning steps were performed in *Escherichia coli* strain DH5a from Invitrogen (Carlsbad, CA). Protein expression was carried out in *E. coli* strain BL21DE3 (Invitrogen, Carlsbad, CA). Kanamicine and imidazole were purchased from Sigma (St. Louis, MO). Silicon wafer chips were obtained from Ted Pella, Inc. (Redding, CA). Other chemicals with the highest grade of purity were purchased from Fisher Scientific (Pittsburg, PA).

Cloning, Expression, and Purification of Spider Silk Block Copolymers

The spider silk block copolymers were constructed and cloned into a commercially available expression pET30a (+) vector in a similar fashion to the procedure we have described previously (Rabotyagova et al., 2009; Tokareva et al., 2013a). The amino acid sequence of the A and B blocks were derived from major ampullate dragline silk I of *N. clavipes* (Accession Number: P19837). The coding sequences of two spider silk-like blocks were AB and AB_3, where are A is a hydrophobic block and B is a hydrophilic block, were designed to carry *SpeI* and *NheI* restriction sites at the ends of the coding sequences for the ligation of the blocks into a modified pET30a (+) vector. By using a step-by-step directional ligation approach, direct control over the assembly of monomeric genes into complex sequences was achieved. Ligation reactions were carried out with T4 DNA ligase (Invitrogen, Carlsbad, CA) at 16°C.

The cloned constructs were transformed into the bacterial host for protein expression. Larger-scale expression was performed using a fermentor (BioFlow3000, New Brunswick Scientific Co., Edison, NJ). Minimal medium supplemented with 1% yeast extract was

employed (Bini et al., 2006). Ammonia was used to maintain the pH at 6.8. When the pH exceeded 6.88 a feed solution (50% glucose, 10% yeast extract, 2% $MgSO_4x7H_2O$) was added. All culture media contained kanamycin (50 μg/mL). Expression was induced by the addition of 1 mM isopropyl β-D-1-thiogalactopyranoside (IPTG) (Fisher Scientific, Hampton, NH) when the optical density, OD_{600} was between 10 and 15.

Protein purification was performed under denaturing conditions on Ni-NTA resins (Qiagen, Valencia, CA) using our previously published procedure (Rabotyagova et al., 2009). The spider silk block copolymers were eluted using urea-based buffer (pH 4.5). The proteins were dialyzed against water using Slide-ALyzer Cassette (Pierce, Rockford, IL) with MWCO of 2,000 Da. Dialyzed proteins were lyophilized. The purity of expressed proteins was verified by sodium dodecyl sulfate polyacrylamide gel electrophoresis (SDS-PAGE) followed by Colloidal Blue staining. Protein identity was confirmed by matrix-assisted laser desorption ionization mass spectrometry (MALDI-TOF; Tufts Core Chemistry Facility, Boston, MA) and amino acid sequencing (MALDI-TOF; Tufts Core Chemistry Facility, Boston, MA).

Dynamic Light Scattering (DLS)

Concentrated and dilute aqueous solutions of spider silk block copolymers were analyzed by DLS (Brookhaven Instruments Corporation, Holtsville, NY). DLS was performed using a 532 nm laser at room temperature with a scattering angle of 90°. To prepare concentrated silk solutions, lyophilized recombinant silk proteins were dissolved in 9.3MLiBr at various concentrations followed by dialysis against DI water.

Scanning Electron Microscopy (SEM)

SEM was used to assess morphological characterization of the spider silk block copolymers. The experiments were performed using a Zeiss 55Ultra and a Zeiss Supra Systems (Harvard University Center for Nanoscale Systems, Cambridge, MA). Lyophilized spider silk block copolymers were dissolved in water to a final concentration of 1 mg/mL and dried on a silicon chip in a closed container at room temperature. Images were taken using InLense and SE2 detectors at 5.00 kV.

Atomic force microscopy (AFM)

AFM imaging and force spectroscopy measurements were performed on an Asylum Research MFP-3D-Bio Atomic Force Microscope (Asylum Research, an Oxford Instruments Company, Santa Barbara, CA). For imaging in fluids, 80 μL sample was deposited as a drop on a silicon substrate and imaged. IgorPro 6.22A image analysis software was used to determine the heights of observed structures. The root-mean-square (rms) and the arithmetic average height (Ra) were determined using software to find differences between roughnesses of samples. All imaging was performed in contact mode using Olympus silicon probes on a silicon surface. Cantilever specifications are the following: 160 μm in length, 40 μm in width, with a resonant frequency of 300±50 kHz.

Fourier Transform Infrared Spectroscopy (FTIR)

The infrared spectra of spider silk-like block copolymers were recorded using a FTIR spectrometer, Jasco FT/IR-6200 (Jasco Instruments, Easton, MD). The measurements were conducted on lyophilized silk samples. Spectra were scanned in absorption mode at 4 cm^{-1} resolution from 4000–400 cm^{-1}. All spectral manipulations were performed with OPUS software (version 5.0) (Mattson Instruments, Madison, WA). Quantification of the secondary structure was based on analyzing the amide I region (1700 – 1600 cm^{-1}). Background absorption was subtracted from the sample spectra to establish baseline. Spectral deconvolution was performed using the procedure described previously (Hu et al., 2006). Briefly, Fourier self-deconvolution (FSD) was performed over the amide I region on the spectra with Lorentzian peak profile (half-bandwidth of 25 cm^{-1} and a noise reduction factor of 0.3). The average secondary structure percent composition of the spider silk block copolymers, in particular, the β-sheet content, was assessed by integrating the area of each deconvoluted curve, and then normalizing to the total area of the amide I peak.

Coarse-Grained Dissipative Particle Dynamics (DPD)

All DPD simulations were carried out using the massively parallelized LAMMPS package (Plimpton, 1995). The simulations were run in a rectangular box ($60 \times 40 \times 40$ R_c^3, where $R_c = 0.9321$ nm is the physical length scale in the DPD model) and periodic boundary conditions. The box size was chosen to be longer than a single extended chain to avoid artifacts from boundary conditions. The concentration of protein was fixed to 20% volume fraction of peptide beads in all cases, where each bead represents three amino acids in a coarse-grained manner. The total number of beads in a system was 288,000. For the starting structure, peptides chains were randomly grown with a fixed distance (where is the equilibrium bond distance in the chain) between beads in the simulation box, up to 20% of the volume fraction. The box was then filled with solvent beads until the number density of 3 was reached. All DPD simulations were run with a fixed time step of $t = 0.03$ τ, where τ = 0.75 ns is the physical time scale in the DPD model. Equilibration simulation was performed until a steady state was achieved by tracking the root-mean-square-deviation (RMSD) for 210,000 time steps. Interested readers can refer to previous publications on the details of the DPD formalism and the parameterization procedure (Groot and Warren, 1997), including the assignment of bead types to the A and B blocks of the copolymer and the interactions parameters (Wong et al., 2012).

Microfluidic Spinning

Aqueous H(AB)$_2$ and H(AB)$_{12}$ solutions of 20% w/v and pH 7.4 were prepared by dissolving bioengineered silk proteins in 9 M LiBr followed by extensive dialysis against water. Poly(ethylene oxide) (PEO) solution of 3% w/v was prepared from 900,000 MW PEO (Sigma Aldrich, St. Louis, MO) in water and hydrochloric acid was used to adjust the solution pH to 1.5. The design and fabrication of the poly(dimethylsiloxane) (PDMS) silk spinning devices has been previously reported (Kinahan et al., 2011). The product was collected in a methanol reservoir and washed in water 3 times.

Results and Discussion

The spider silk block copolymers were prepared based on the assembly of two individual blocks, a hydrophobic poly-alanine rich block (A) and a hydrophilic glycine-rich block (B) (Rabotyagova et al., 2009). The A block consisted of one poly(GA) repeat (GAGAAAAAGGAG) responsible for β-sheet formation. The B block was composed of four GGX repeats, separated by the GSQGSGR sequence (Table 1). Figure 1 depicts the cloning strategy to bioengineer the recombinant spider silk block copolymers. Table 1 shows the spider silk block copolymer amino acid sequences prepared for this study.

The concept behind the block design is the ability of hydrophobic segments (A blocks) to pack together, while exposed to water, since this would be entropically favorable. At the same time, the hydrophilic segments (B blocks) favorably dissolve in water. In block copolymers prepared by covalent bonding of thermodynamically incompatible blocks, macroscopic phase separation cannot take place; instead, microscopic separation occurs in bulk and in solution resulting in the formation of different structures (e.g., lamellae, hexagonally packed cylinders, spheres). The observed microstructures are the result of a compromise between mixing and separation. The length scale of the microstructures is comparable to the size of the silk block copolymers (5–100 nm); therefore, the microstructures possess all of the chemical and physical characteristics of spider silks (Rabotyagova et al., 2011). Block copolymer phase behavior is primarily determined by three parameters: the overall degree of polymerization N, the volume fraction of hydrophobic block A (f_A), and the Flory-Huggins segment-segment interaction parameter (χ). The Flory-Huggins interaction parameter is an essential parameter in block copolymer theory since it provides the driving force for the phase separation (Hadjichristidis et al., 2003). This parameter describes the free energy cost per monomer in a situation when two unlike units want to segregate. However, polydispersity seems to lead to shifting phase boundaries and increases the domain spacing as a result of different chain lengths. An increase in domain spacing was detected when morphologies were observed by AFM and micelle sizes measured by DLS for the $H(AB)_2$ and $H(AB)_{12}$ silk block copolymers (Figure 2) were compared. $H(AB)_2$ self-assembled into small micelles in dilute solution (0.25 mg/ml) with an average diameter of 2 nm±0.5 nm; whereas, $H(AB)_{12}$ formed larger micelles with an average diameter of 32 nm±5 nm at the same concentration. The simulation results (Figure 2) are consistent with the experimentally observed trends in which $H(AB)_{12}$ formed larger spherical aggregates with a diameter of ~10 nm; whereas $H(AB)_2$ formed smaller spherical aggregates with an averaged diameter of ~5 nm.

The two proteins demonstrated similar morphological features (*i.e.*, spherical aggregates) in solution but not upon drying. SEM images of the assemblies formed from solution concentrations of 1 mg/ml (A, C) and 2.5 mg/ml (B, D) revealed that $H(AB)_2$ formed films of spherical aggregates, while $H(AB)_{12}$ selfassembled into nano-fibrils upon drying at both concentrations (Figure 3). The diameter of the observed $H(AB)_{12}$ nano-fibrils increased with increase in protein concentration. $H(AB)_2$ formed films of spherical aggregates. This observation further supports the importance of the number of repetitive blocks (e.g., chain length) related to fiber formation.

At high concentration (100 mg/ml), H(AB)$_{12}$ formed hierarchically organized self-assembled structures upon evaporation of the aqueous solvent, suggesting an important role that protein concentration plays in the organized microstructures formation process. With an increase in protein concentration up to 200 mg/ml liquid-liquid phase separation of a protein-rich phase and a protein-poor phase occurred upon drying, resulting in the formation of organized lamellar microstructures. Horizontally aligned lamellar structures, organized into periodic assemblies with an average width of 5 ± 1 μm, were formed (Figure 4). Horizontally aligned lamellar structures organized into periodic assemblies with an average width of 5 ± 1 μm were formed (Figure 4). The formation of the organized periodic assemblies of recombinant silks at high concentration is a promising step towards the fiber formation process indicating that important structural alignment steps took place. It should be noted that almost all recombinantly produced spidroins show low solubility in aqueous solution and tend to aggregate into non-organized small fibrillar structures as a result of inadequate self-assembly (Eisoldt et al., 2011).

Lamellar microstructures formation can be induced by applying shear forces leading to alignment of β-sheet-rich regions and ultimately, polymeric network formation. Thus, based on this insight, shear was applied experimentally to the aqueous protein solutions of H(AB)$_2$ and H(AB)$_{12}$ to induce polymeric network formation and ultimately, formation of the solid material.

Using a microfluidic channel, a solid H(AB)$_{12}$ film was formed from 20% w/v block copolymer solution. No solid material was observed when H(AB)$_2$ was spun at the same concentration. The formation of the solid material can be explained by differences in the length of the engineered spider silks, since H(AB)$_2$ has fewer blocks than H(AB)$_{12}$. This further indicates that the length of the spider silk block copolymer significantly affects the ability to form structured, polymeric networks that assemble into mechanically robust materials. Under shear flow, polymer chains extended along the shear flow direction and the size of aggregates increased by merging multiple micelles.

SEM images revealed that spun H(AB)$_{12}$ films were composed of nano-fibrillar assemblies with a diameter around 25 nm (Figure 5). The mechanism for the H(AB)$_{12}$ nano-fibrillar network formation is likely based on the alignment of the β-sheet forming poly-alanine regions with normals to the sheets lying along the shear direction. These fibrils formed under shear as a result of the hierarchical self-assembly of β-strands into lamellar microstructures that self-organized into woven nano-fibrillar assemblies that form the solid films. The effect of shear was not observed in the case of H(AB)$_2$.

Films prepared from spun H(AB)$_{12}$ and non-spun H(AB)$_2$ and H(AB)$_{12}$ spider silk block copolymers were assessed for differences in secondary structure by FTIR–ATR (Figure 6). The frequency from 1700 to 1400 cm^{-1} contains the most important amide I and amide II regions [49]. The amide I band has strong absorption at 1700–1600 cm^{-1} (Monti et al., 1998), from the C=O stretching vibration (80%) with minor contributions from N-H in plane bending, out of phase C-N stretching vibrations, and C-N deformation (Hu et al., 2006; Rabotyagova et al., 2010). The amide I vibration is generally not affected by the nature of the side chains; therefore, it is most commonly used for analysis of secondary structure.

Characteristic assignments of distinct peaks for spider silk were made in accordance with previously published reports (Krishnaji et al., 2013; Rabotyagova et al., 2010). After deconvolution, several characteristic peaks were observed. Peaks in the regions 1625 cm^{-1} and 1695 cm^{-1} indicated the presence of β-sheets, 1635–1650 cm^{-1} correspond to random coils, 1655–1660 cm^{-1} represented α– helices and 1668–1690 cm^{-1} corresponded to β–turns. In the case of non-spun films, FTIR indicated that the random coil conformation was the dominant secondary structure for both spider silk block copolymers. The percentages of the helical conformation were 13% and 11% for H(AB)$_2$ and H(AB)$_{12}$, respectively, and the β-sheet content was similar for both polymers and estimated at 8 % (Figure 6). When FTIR spectra of spun H(AB)$_{12}$ films were compared to their non-spun counterparts, a significant shift from 1645 cm^{-1} to lower wavenumber, 1625 cm^{-1}, was observed together with the appearance of a shoulder peak at 1695 cm^{-1}. These changes indicate the presence of anti-parallel β-sheets in the spun H(AB)$_{12}$ film. Deconvolution revealed a significant increase in the β-sheet content of the spun H(AB)$_{12}$ films that changed from 8% to 40% a concomitant decrease in the random coil conformation that changed from 50% to 22% (Figure 6). In addition to wavenumber shifts observed in amide I and amide II regions, spectra of the spun H(AB)$_{12}$ films have a sharp non-overlapping peak at 963 ± 2 cm^{-1} corresponding to a coupled side-chain and main-chain stretching vibration (Papadopoulos et al., 2007). This lower wavenumber peak is assigned to poly-alanine β-sheets (Anton et al., 2013). In the case of the non-spun H(AB)$_{12}$ and H(AB)$_2$ films, this lower wavenumber peak is not present. The increase in the β-sheet content is indicative of the irreversible changes that occur in the secondary structure of spider silk block copolymers upon administration of shear flow, indicating further that nano-fibrillar assemblies are formed from β-strand alignment into the β-sheet-rich regions.

When 2M potassium phosphate was included in the solution, smooth, round microspheres were formed from H(AB)$_{12}$ (Figure 7). H(AB)$_2$ did not from any organized structures under these conditions. Microspheres are an example of a non-natural material format made of silk proteins that can be used for incorporation of drugs. Additionally, the surface of these structures can be further functionalized with signal molecules/peptides for site-specific targeting.

High concentrations of salts can precipitate proteins by "salting-out" (Voet and Voet, 2005). The nature of the ions can impact the process as described by the Hofmeister series (Hardy and Scheibel, 2010). Potassium phosphate is a strong kosmotropic agent that is highly hydrated. Its hydration shell removes water molecules from a hydrophobic domain leading to dense packing of protein chains and subsequent precipitation. In silks the salting-out process is accompanied by irreversible structural conversion of random coils into organized β-sheets. Based on our previous studies we propose that engineered spider silk microspheres have a core-shell structure with a shell consisting of organized β-sheets and β-turns and a core of 3$_{10}$-helices and random coils (Neubauer et al., 2013; Rabotyagova et al., 2010). Nonorganized morphologies were observed in the case of H(AB)$_2$ under the same conditions, likely due to the inability of short hydrophobic domains to form stable packing arrangements.

Conclusions

Two spider silk block copolymers were designed, cloned, expressed, and purified and secondary structures and morphologies assessed by FTIR, SEM and AFM. As the number of AB repeats increased, the transformation of the proteins from disordered to lamellar structures occurred. $H(AB)_{12}$ with a Mw of 43.7 kDa self-assembled into nano-fibrillar assemblies with an average diameter of 25 nm in aqueous media; whereas, $H(AB)_2$ with a Mw of 11.6 kDa did not form these morphologies. Using a microfluidic channel, a solid $H(AB)_{12}$ film was formed in solution. SEM analysis revealed that β-sheet-rich lamellar microstructures were precursors to film formation. The experimental findings further demonstrated importance of the protein chain length to regulate material features.

Acknowledgments

References

An B, Jenkins JE, Sampath S, Holland GP, Hinman M, Yarger JL, Lewis R. Reproducing natural spider silks' copolymer behavior in synthetic silk mimics. Biomacromolecules. 2012; 13:3938–3948. [PubMed: 23110450]

Anton AM, Kossack W, Gutsche C, Figuli R, Papadopoulos P, Ebad-Allah J, Kuntscher C, Kremer F. Pressure-Dependent FTIR-Spectroscopy on the Counterbalance between External and Internal Constraints in Spider Silk of Nephila pilipes. Macromolecules. 2013; 46:4919–4923.

Bini E, Wang Po, Foo C, Huang J, Karageorgiou V, Kitchel B, Kaplan DL. RGD-functionalized bioengineered spider dragline silk biomaterial. Biomacromolecules. 2006; 7:3139–3145. [PubMed: 17096543]

Eisoldt L, Smith A, Scheibel T. Decoding the secrets of spider silk. Materials Today. 2011; 14:80–86.

Gosline J, Guerette P, Ortlepp C, Savage K. The mechanical design of spider silks: from fibroin sequence to mechanical function. J Exp Biol. 1999; 202:3295–3303. [PubMed: 10562512]

Gosline JM, Denny MW, DeMont ME. Spider silk as rubber. Nature. 1984; 309:551–552.

Groot RD, Warren PB. Dissipative particle dynamics: Bridging the gap between atomistic and mesoscopic simulation. Journal of Chemical Physics. 1997; 107:4423.

Hardy JG, Scheibel TR. Composite materials based on silk proteins. Progress in Polymer Science. 2010; 35:1093–1115.

Hu X, Kaplan D, Cebe P. Determining β-sheet crystallinity in fibrous proteins by thermal analysis and infrared spectroscopy. Macromolecules. 2006; 39:6161–6170.

Kinahan ME, Filippidi E, Koster S, Hu X, Evans HM, Pfohl T, Kaplan DL, Wong J. Tunable silk: using microfluidics to fabricate silk fibers with controllable properties. Biomacromolecules. 2011; 12:1504–1511. [PubMed: 21438624]

Krishnaji ST, Bratzel G, Kinahan ME, Kluge JA, Staii C, Wong JY, Buehler MJ, Kaplan DL. Sequence–structure–property relationships of recombinant spider silk proteins: integration of biopolymer design, processing, and modeling. Advanced Functional Materials. 2013; 23:241–253.

Lewis RV. Spider silk: ancient ideas for new biomaterials. Chemical Reviews. 2006; 106:3762–3774. [PubMed: 16967919]

Mai Y, Eisenberg A. Self-assembly of block copolymers. Chemical Society Reviews. 2012; 41:5969–5985. [PubMed: 22776960]

Matsen MW, Schick M. Stable and unstable phases of a diblock copolymer melt. Physical Review Letters. 1994; 72:2660–2663. [PubMed: 10055940]

Monti P, Smith G, Bertoluzza A, Kasai T, Tsukada M. Raman spectroscopic studies of silk fibroin from Bombyx mori. Journal of Raman Spectroscopy. 1998; 29:297–304.

Neubauer MP, Blum C, Agostini E, Engert J, Scheibel T, Fery A. Micromechanical characterization of spider silk particles. Biomaterials Science. 2013; 1:1160–1165.

Papadopoulos P, Solter J, Kremer F. Structure-property relationships in major ampullate spider silk as deduced from polarized FTIR spectroscopy. Eur. Phys. J. E. 2007; 24:193–199. [PubMed: 17985073]

Plimpton S. Fast parallel algorithms for short-range molecular dynamics. Journal of Computational Physics. 1995; 117:1–19.

Rabotyagova OS, Cebe P, Kaplan DL. Self-assembly of genetically engineered spider silk block copolymers. Biomacromolecules. 2009; 10:229–236. [PubMed: 19128057]

Rabotyagova OS, Cebe P, Kaplan DL. Role of polyalanine domains in β-sheet formation in spider silk block copolymers. Macromolecular Bioscience. 2010; 10:49–59. [PubMed: 19890885]

Rabotyagova OS, Cebe P, Kaplan DL. Protein-based block copolymers. Biomacromolecules. 2011; 12:269–289. [PubMed: 21235251]

Tokareva O, Michalczechen-Lacerda VA, Rech EL, Kaplan DL. Recombinant DNA production of spider silk proteins. Microbial Biotechnology. 2013a; 6:651–663. [PubMed: 24119078]

Tokareva O, Jacobsen M, Buehler M, Wong J, Kaplan DL. Structure–function–property– design interplay in biopolymers: Spider silk. Acta Biomaterialia. 2013b

Voet, D.; Voet, JG. Biochemistry. 3rd ed.. Wiley and Sons, Inc.; 2005.

Wong JY, McDonald J, Taylor-Pinney M, Spivak DI, Kaplan DL, Buehler MJ. Materials by design: Merging proteins and music. Nano Today. 2012; 7:488–495. [PubMed: 23997808]
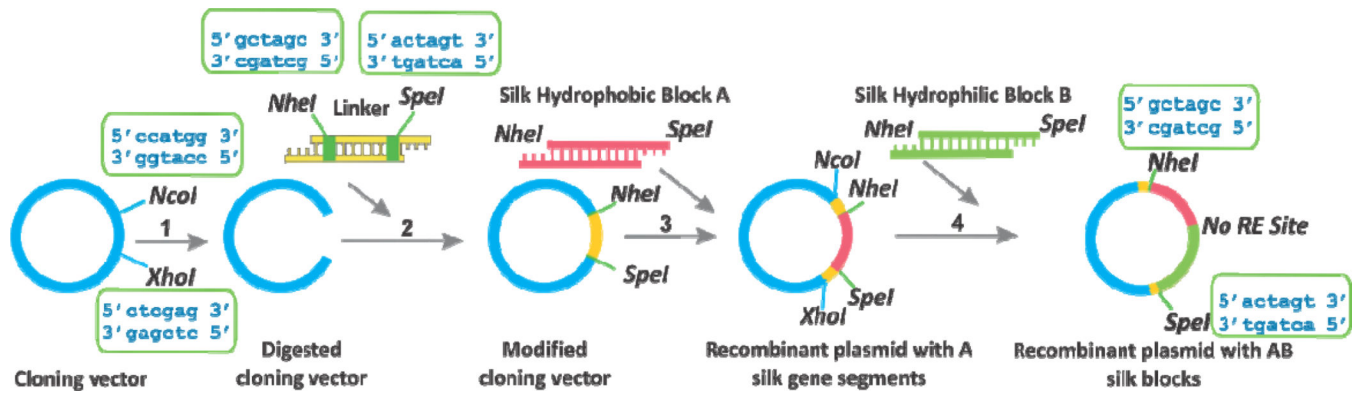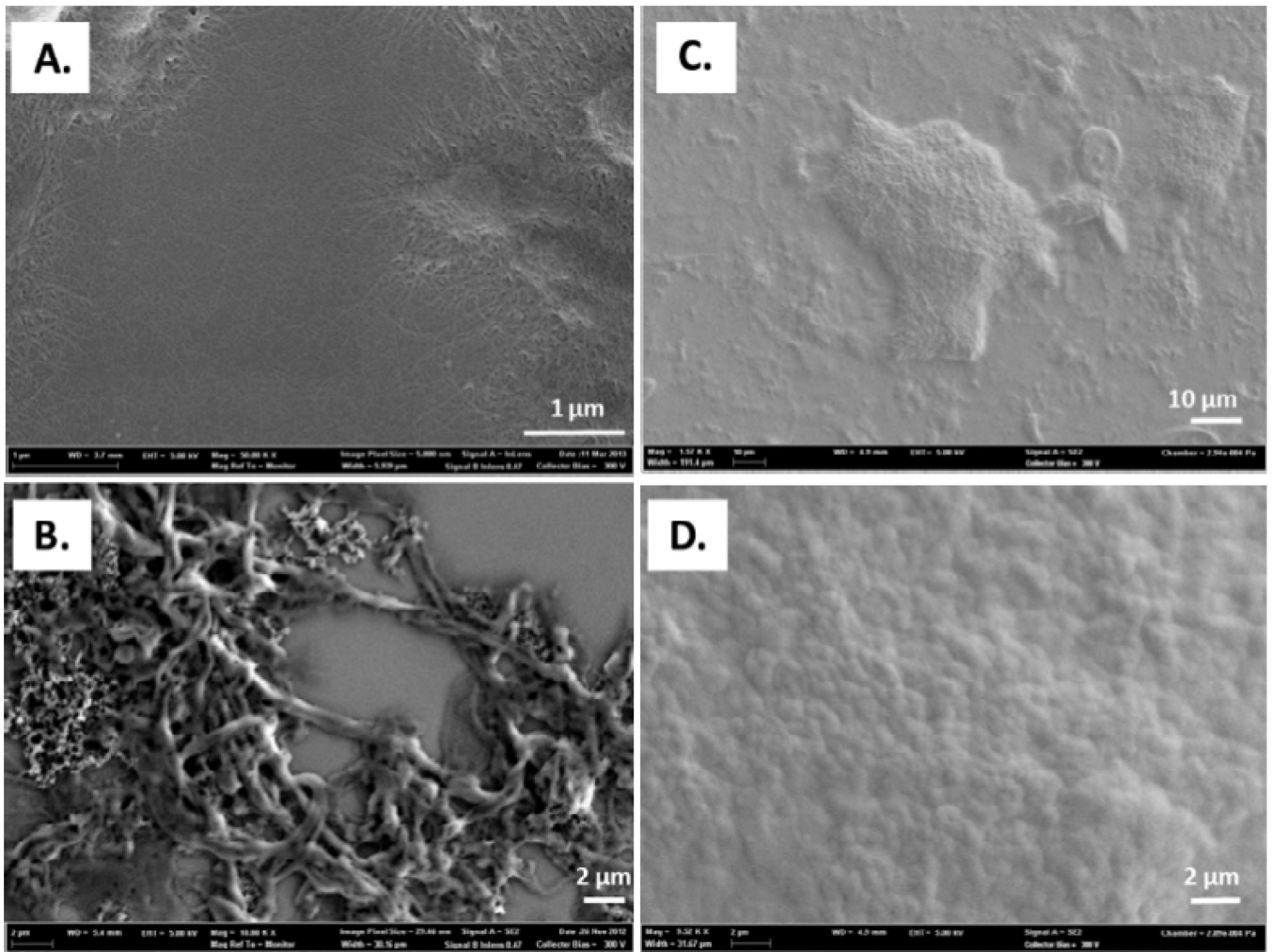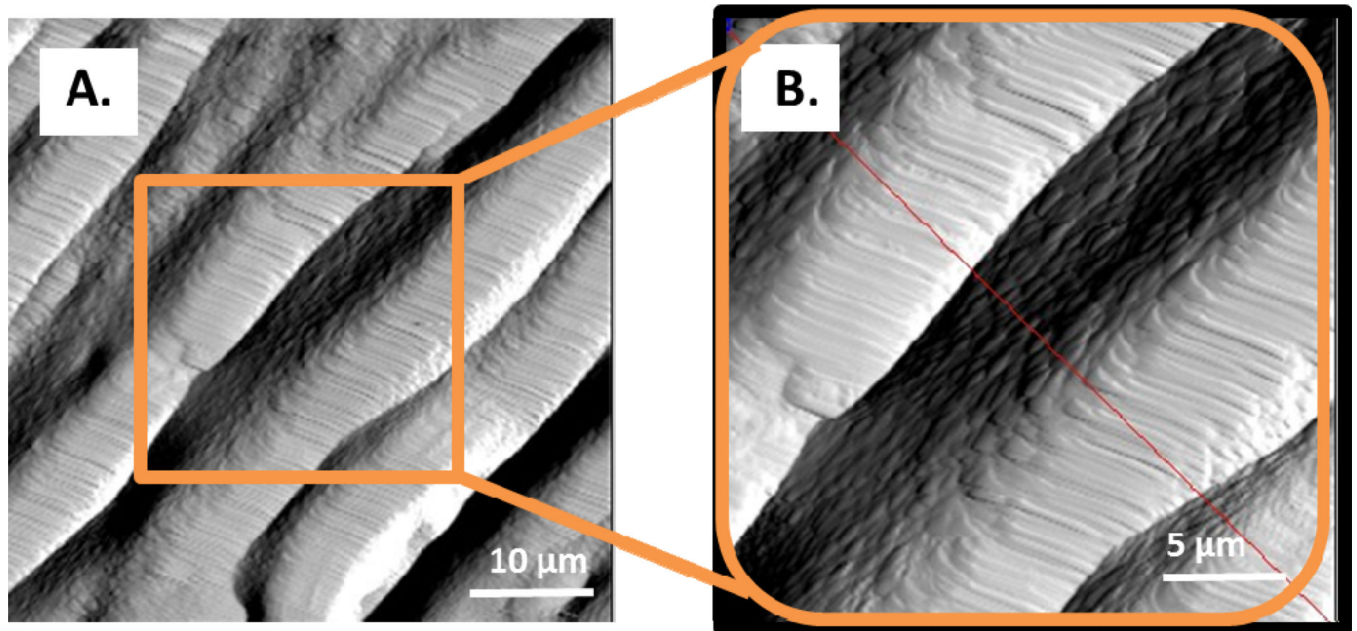
Figure 1.
Schematic representation of the recombinant DNA strategy used to make spider silk block copolymers for the study. *NcoI, NheI, SpeI, XhoI* are restriction enzymes (RE). A box above/ below a specific RE indicates an oligonucleotide sequence recognized by this RE. pet30a(+) plasmid is in blue, cloning linker is in yellow, silk hydrophobic block A is in magenta, and silk hydrophilic block B is in green. Steps are the following: (1) digestion, (2) ligation of a linker, (3) ligation of A block, (4) ligation of B block.
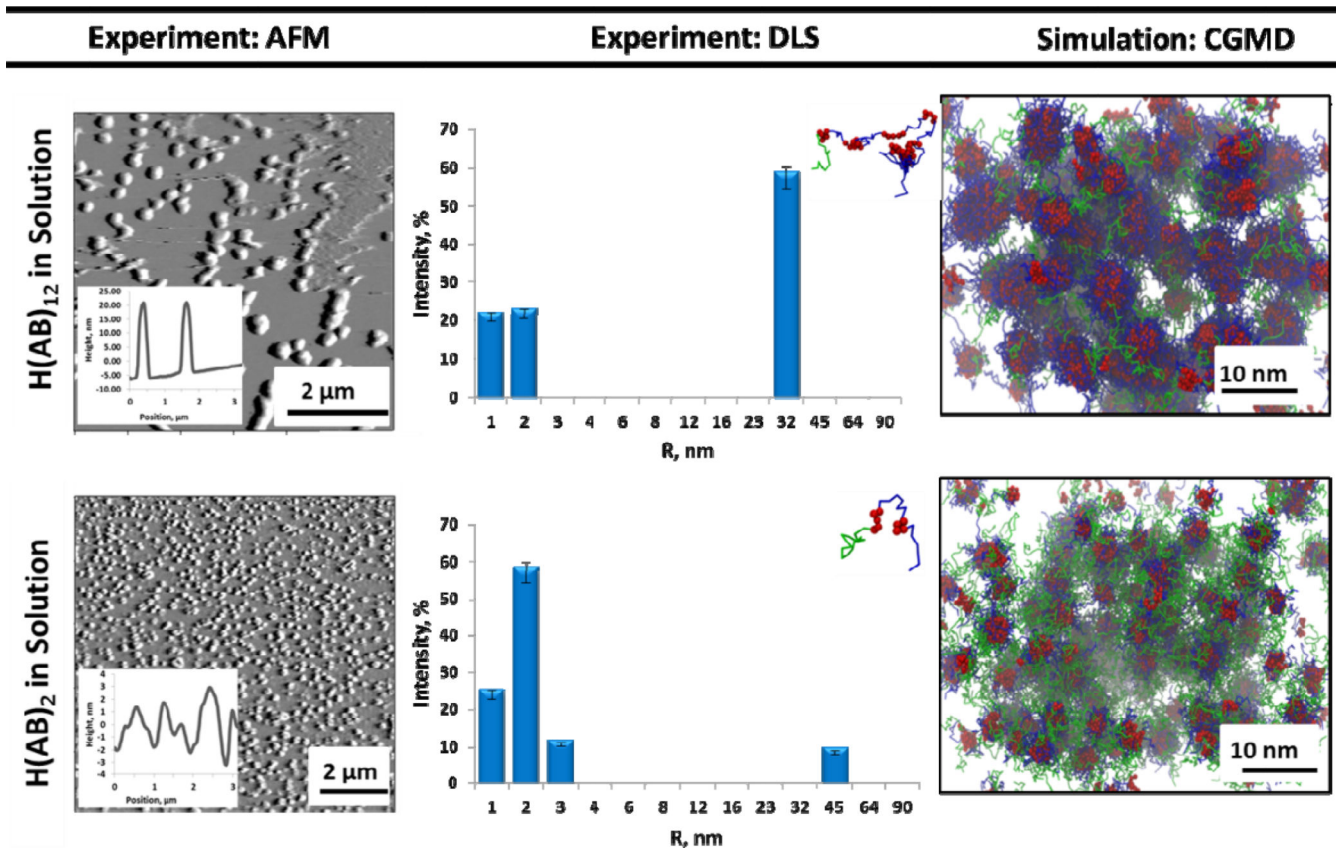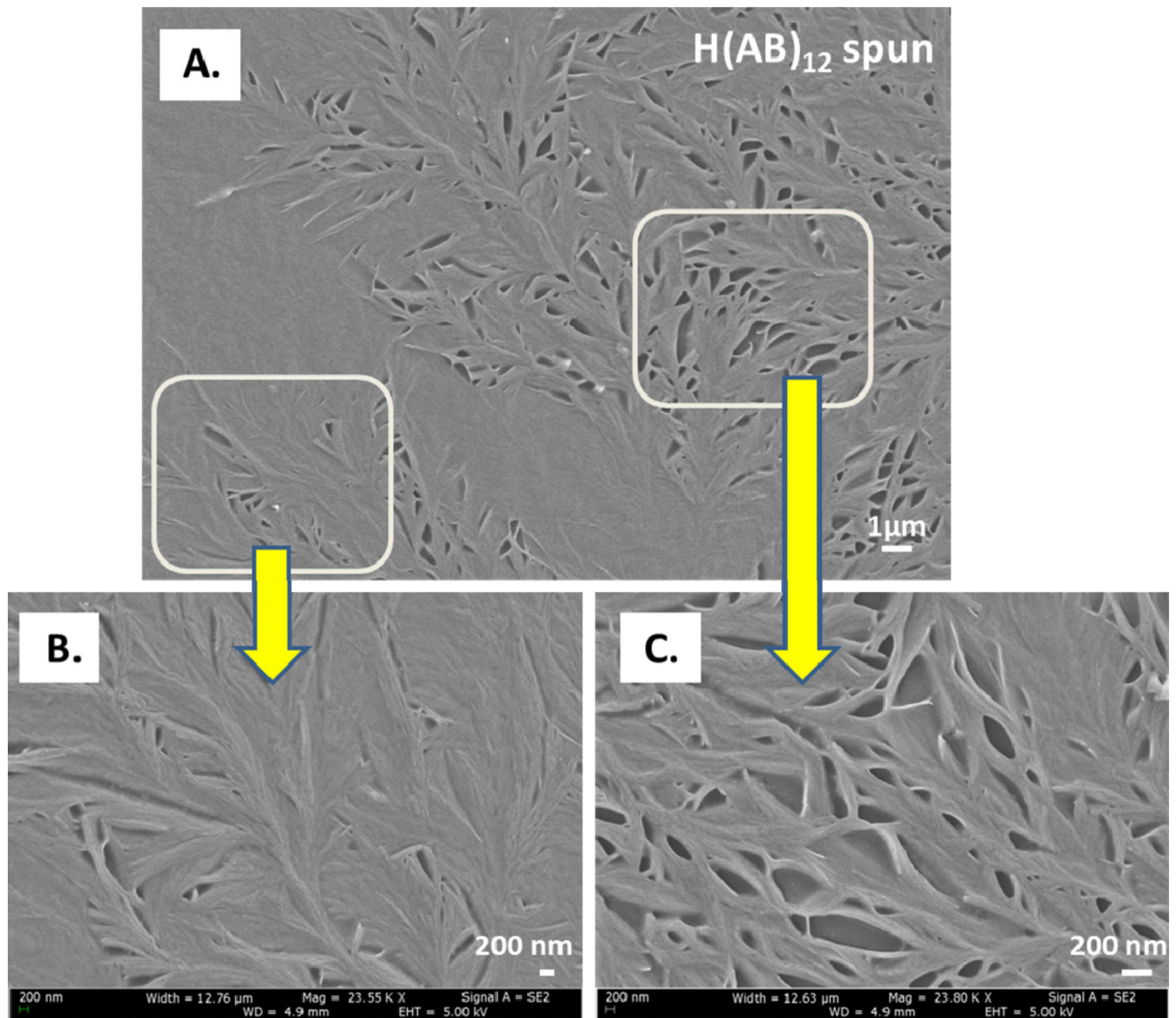
Figure 2.

Comparison among AFM, DLS, and coarse-grained molecular dynamic (CGMD) simulation results on aggregate morphologies of $H(AB)_{12}$ and $H(AB)_2$ recombinant spider silk block copolymers in aqueous solution. Experimental panel (AFM and DLS) depicts that $H(AB)_{12}$ formed larger micelles with an average diameter of 32 nm ± 5 nm and $H(AB)_2$ self-assembled into smaller micelles with an average diameter of 2 nm ± 0.5 nm. For both types of spider silk block copolymers, micelles were observed at concentration of 0.25 mg/ml in aqueous media. The simulation results (simulation panel) depicts formation of the small spherical aggregates in the case of $H(AB)_2$ and large spherical aggregates in the case of $H(AB)_{12}$.
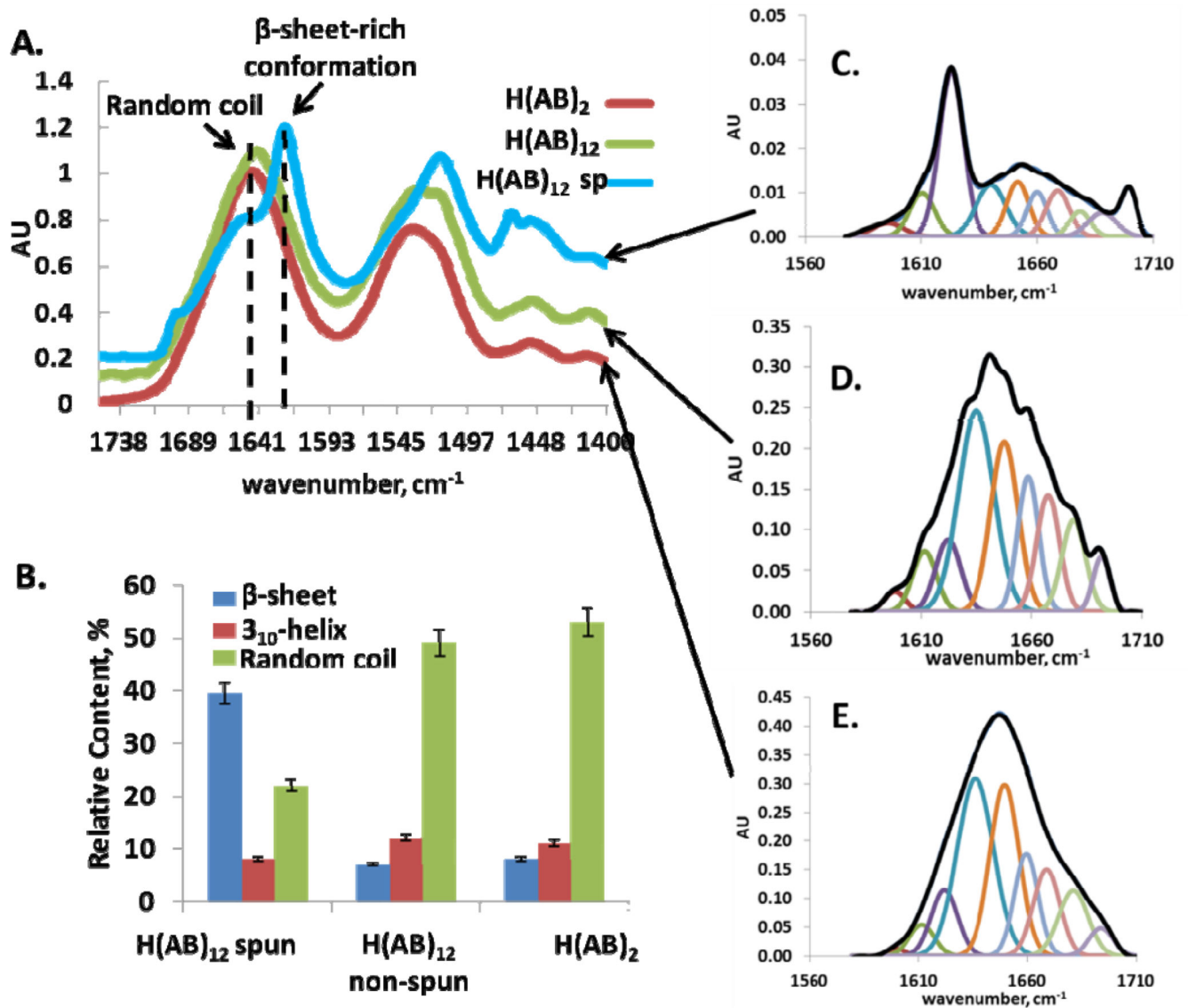
Figure 3.
SEM images of H(AB)$_{12}$ and H(AB)$_2$ at 1 mg/ml (A, C) and 2.5 mg/ml (B, D), respectively. Nanofibrils (A) and fibrils (B) were observed for H(AB)$_{12}$. Film formation was observed for H(AB)$_2$ (C, D).
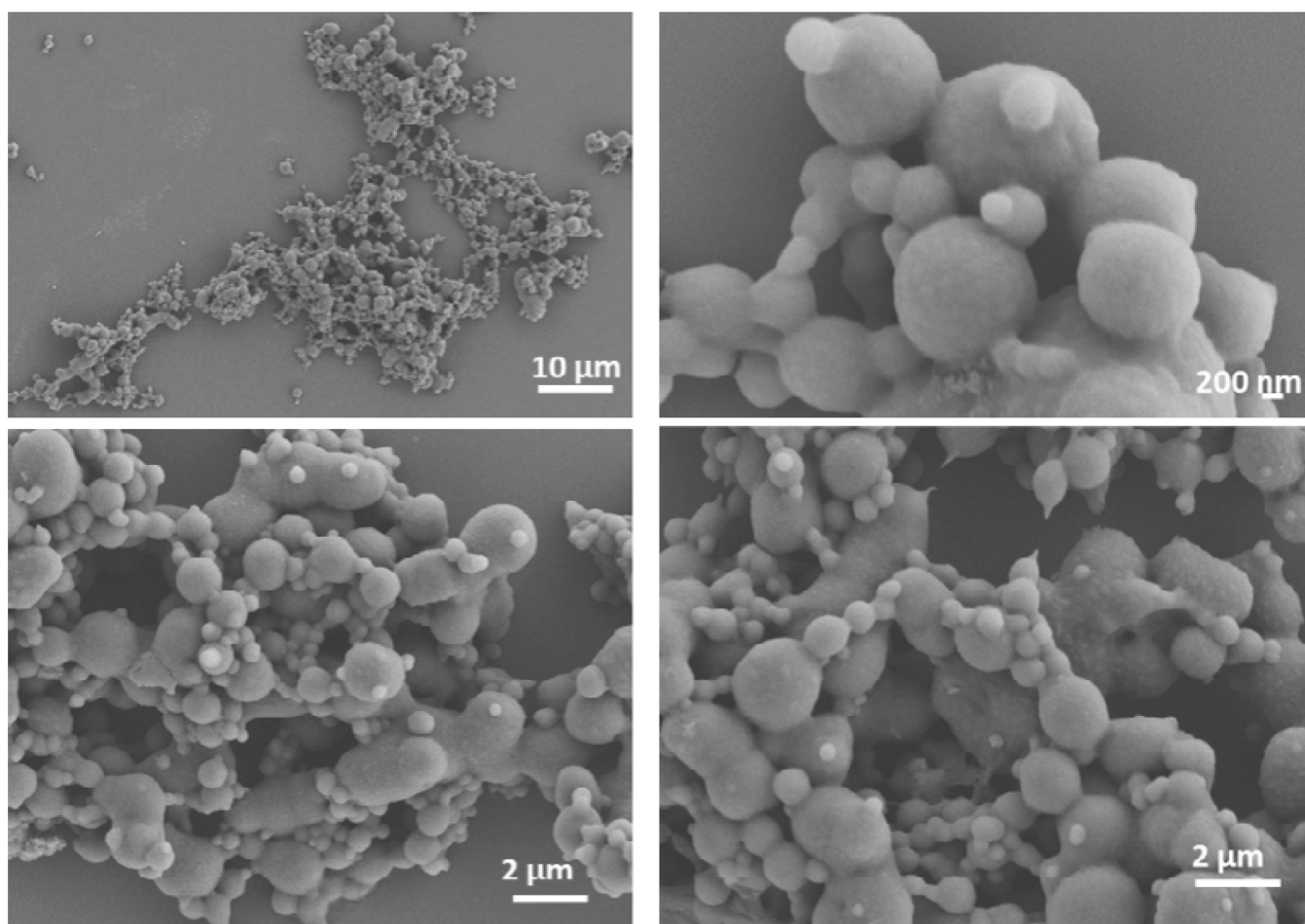
Figure 4.
(A) AFM deflection image of 10% w/v $H(AB)_{12}$. (B) The zoomed-in AFM deflection image of the selected section (in orange). Both images demonstrate hierarchical assemblies. 10% w/v $H(AB)_{12}$ aqueous solution was prepared as described in the experimental section and deposited on a clean silicon wafer. Upon drying periodic lamellar stacks were observed.

Figure 5.
(A) SEM spun H(AB)$_{12}$ at 20% w/v. (B, C) Nano-fibrillar assemblies were observed for spun H(AB)$_{12}$ film. H(AB)$_{12}$ film was washed with water, air dried, and imaged at 5kV. The film is composed of densely-packed and loosely-packed regions of interwoven nano-fibrils.

Figure 6.
(A) FTIR Absorbance of spun $H(AB)_{12}$ (blue), non-spun $H(AB)_{12}$ (green), and non-spun $H(AB)_2$ (red) spider silk block copolymers. (B) Relative percentages of β-sheet-rich (blue), 3_{10}-helical (red), and random coil secondary structures (green). (C, D, and E) Fourier self-deconvolution of amide I spun $H(AB)_{12}$ (C), non-spun $H(AB)_{12}$ (D), and non-spun $H(AB)_2$ (E). Key: heavy black line, measured data; thin solid lines, individual Gaussian peaks.

Figure 7.
SEM images of H(AB)$_{12}$ microshperes formed in the presence of 2M potassium phosphate at different magnifications.

Table 1

The spider silk block copolymers prepared for this study.

Name	Sequence	Mw, Da	PI
H(AB)₂	M H H H H H H S S G L V P R G S G M K E T A A A K F E R Q H M D S P D L G T D D D D K A M A A S R G G G Y A G A G A A A A A G G A G A A Q G G Y G G L G S Q G S G R G G L G G Q A A G A G A A A A A G G A G A A Q G G Y G G L G S Q G S G R G G L G G Q A A A T S	11,654	7.06
H(AB)₁₂	M H H H H H H S S G L V P R G S G M K E T A A A K F E R Q H M D S P D L G T D D D D K A M A A S R G G G Y A G A G A A A A A G G A G A A Q G G Y G G L G S Q G S G R G G L G G Q A A G A G A A A A A G G A G A A Q G G Y G G L G S Q G S G R G G L G G Q A A A T S R G G G Y A G A G A A A A A G G A G A A Q G G Y G G L G S Q G S G R G G L G G Q A A G A G A A A A A G G A G A A Q G G Y G G L G S Q G S G R G G L G G Q A A A T S R G G G Y A G A G A A A A A G G A G A A Q G G Y G G L G S Q G S G R G G L G G Q A A G A G A A A A A G G A G A A Q G G Y G G L G S Q G S G R G G L G G Q A A A T S R G G G Y A G A G A A A A A G G A G A A Q G G Y G G L G S Q G S G R G G L G G Q A A G A G A A A A A G G A G A A Q G G Y G G L G S Q G S G R G G L G G Q A A A T S R G G G Y A G A G A A A A A G G A G A A Q G G Y G G L G S Q G S G R G G L G G Q A A A T S	43,748	10.27